



## Blocking systems over an aqua planet

Yongyun Hu,<sup>1</sup> Da Yang,<sup>1</sup> and Jun Yang<sup>1</sup>

Received 15 July 2008; revised 31 August 2008; accepted 9 September 2008; published 10 October 2008.

[1] It is well established that forced planetary waves are critically important for blocking formation. To test whether blocking can be generated and maintained in the absence of topographic forcing, we carry out aqua-planet simulations using NCAR CAM2. Results show that blockings occur frequently under the aqua-planet conditions which have no forcing such as land-sea contrast, orography and stationary remote tropical forcing. Features of simulated blockings well resemble that in the real atmosphere, showing typical  $\Omega$ -like patterns, persistence, and quasi-stationary behavior with occasionally westward shifting. It is found that the onset and maintenance of simulated blockings are due to interaction between quasi-stationary free Rossby waves and baroclinic eddies. For 10-year simulations, the blocking frequency is slightly higher than that in the Northern Hemisphere (NH) in the real atmosphere. These suggest that blocking is a natural consequence of rotating and baroclinic atmospheres, while locally topographic forcing and remote tropical forcing are not necessary conditions. **Citation:** Hu, Y., D. Yang, and J. Yang (2008), Blocking systems over an aqua planet, *Geophys. Res. Lett.*, 35, L19818, doi:10.1029/2008GL035351.

### 1. Introduction

[2] Atmospheric blocking is a term denoting anomalously large-amplitude ridge highs (anticyclones) at middle and high latitudes, which are quasi-stationary and unusually persistent. During a blocking episode, the usual eastward propagation of weather systems is obstructed, and cold polar air outbreaks and intrudes in the extratropics. Due to the importance of blocking in weather forecasting, understanding the mechanisms of onset and maintenance of blocking has been of primary interest for research in synoptic and dynamic meteorology for many decades. It is generally thought that forced quasi-stationary planetary waves by land-sea contrast and orography are critically important in the onset and maintenance of blocking.

[3] In their pioneer work, *Charney and DeVore* [1979] suggested that blocking can be generated from the resonant response of large-scale waves to orographic forcing. *Tung and Lindzen* [1979] showed that blocking can be explained through linear resonance of forced planetary-scale waves. It was later recognized that transient baroclinic eddies play important roles in forcing and maintaining blocking throughout interaction with forced quasi-stationary planetary waves [*Hansen and Chen*, 1982; *Hoskins et al.*, 1983; *Egger et al.*, 1986; *Shutts*, 1986; *Dole*, 1986; *Mullen*, 1987;

*Nakamura et al.*, 1997; *Chang et al.*, 2002; *Luo and Chen*, 2006]. These works showed that poleward advection of anticyclonic vorticity and upscale energy cascade by transient eddies maintain blocking highs against dissipation forces. Although the importance of baroclinic transient eddies was greatly emphasized in these later studies, forced planetary waves are still considered a necessary condition for the onset and maintenance of blocking systems.

[4] In addition to local topographic forcing, remote forcing from the tropics was also thought to be an important factor for blocking formation, throughout atmospheric teleconnections. *Renwick and Wallace* [1996] found a statistically significant relationship between El Niño-Southern Oscillation (ENSO) variability and the frequency of wintertime blocking events over northeastern Pacific, that is, the frequency of blocking events is lower during the warm phase of ENSO (El Niño) and higher in the cool phase (La Niña).

[5] While the mechanisms proposed in the above works can adequately explain the formation and location preference of observed blockings, it is not clear whether blocking can be generated in the absence of local topographic forcing and remote tropical forcing. To explore the question, we carry out general circulation model (GCM) simulations under idealized aqua-planet boundary condition, which has a zonally uniform sea surface, along with meridionally varying sea surface temperatures (SST). As pointed out by *Feldstein and Lee* [1996], the aqua-planet model has advantages that the lower atmospheric boundary is smooth and time-independent and that the model retains all the physical parameterizations of a full GCM.

### 2. Model and Simulation Setup

[6] The model used here is the Community Atmosphere Model (CAM2) developed at the National Center for Atmospheric Research [*Collins et al.*, 2003]. It has horizontal resolution of approximately  $2.8^\circ \times 2.8^\circ$  in latitude and longitude and 26 vertical levels from the surface to 2.917 hPa. Simulation setup is same as the control experiment of aqua-planet simulations by *Neale and Hoskins* [2001a, 2001b], that is, the CAM2 is forced by zonally uniform SST distributions varying in latitude only, with a maximum value of  $27^\circ\text{C}$  at the equator and constant values of  $0^\circ\text{C}$  at poleward of both  $60^\circ\text{N}$  and S (sea-ice switched off). Since the insolation is fixed at March equinoctial conditions, there are no seasonal variations. As pointed out by *Neale and Hoskins* [2001a, 2001b], the simulation generates greater latitudinal temperature gradients than observed and the largest temperature gradient is confined closer to the equator, although the simulated thermal structures resemble observations. Consistent with the thermal structures, subtropical jets are also stronger and closer to the

<sup>1</sup>Department of Atmospheric Sciences, School of Physics, Peking University, Beijing, China.

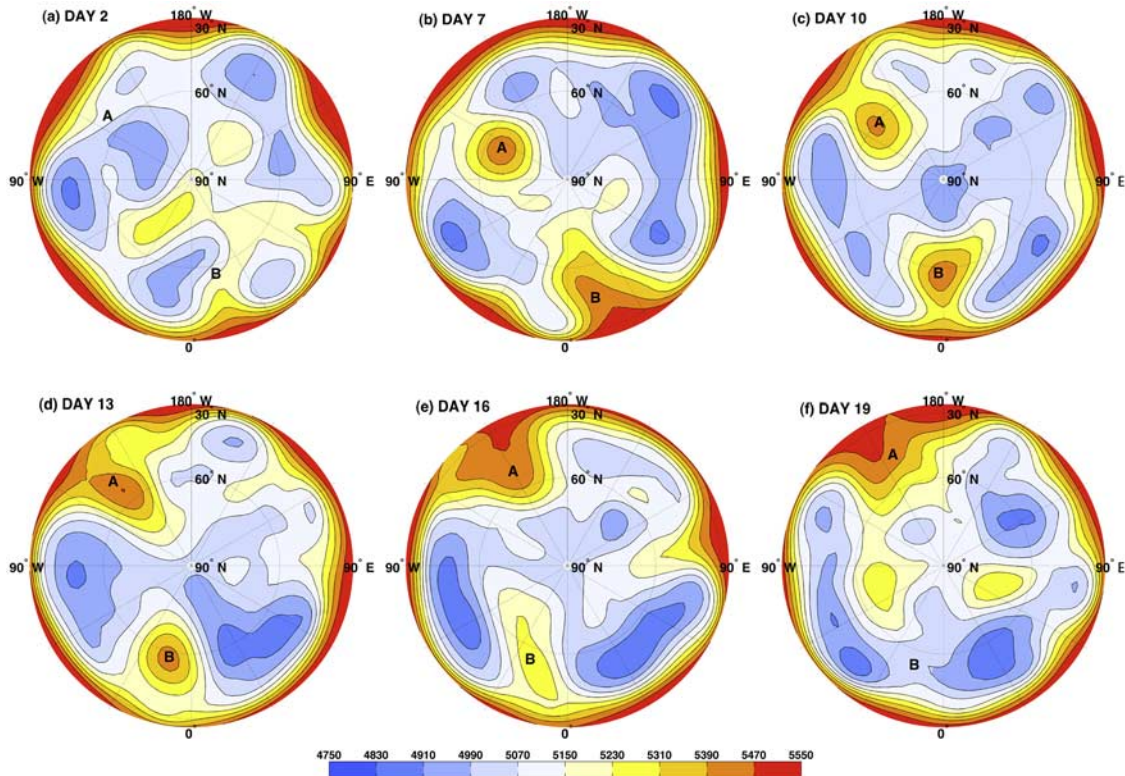


**Figure 1.** Snapshots of 500 hPa geopotential heights during two blocking episodes. The maps range from 20°N to 90°N. Color interval is 80 m.

equator than observed. The model is run for 15 years. The last 10-year results are used for analysis.

### 3. Results

[7] Figure 1 shows snapshots of geopotential heights at 500 hPa over a period with two blocking episodes. At day 2, the geopotential field shows a spatial pattern of wave-number 5 or 6. The two weak ridges, marked by A and B, respectively, will develop into blocking highs and are what we are interested in. Ridge A develops into a  $\Omega$ -like anticyclone by day 7. The anticyclone centers in the north of 60°N, with a cut-off low at each side. Ridge B becomes a  $\Omega$ -like anticyclone at day 10. At day 13, ridge A retreats from the  $\Omega$ -like pattern to a ridge high, while ridge B retains its  $\Omega$ -like pattern. Both ridges show weakening tendency at day 16. By day 19, ridge B disappears, while ridge A remains with a weaker amplitude. In many aspects, the two ridges resemble the typical blocking pattern observed in the real atmosphere. First, they all show anomalously large amplitudes. Especially, they display  $\Omega$ -like patterns at their matured stage. Second, they all show unusual persistence, lasting for about two weeks. Third, they all show quasi-stationary behavior with slow westward shifting. Note that there is another blocking occurring between 120°E and 150°E around day 25.

[8] To examine how the simulated blockings are generated and maintained, we use a 7-day time filter to separate the geopotential height field at 500 hPa into high- and low-pass components. Figures 2a, 2b, and 2c show the high-pass filtered geopotential heights at 500 hPa (color shading)

superimposed on the low-pass filtered geopotential heights at the same level (contours) for days 2, 10, 16, respectively, which represent the onset, maintenance and decaying stages of the blocking episodes in Figure 1. In Figure 2a, the low-pass component roughly shows a zonal wave-number 5 pattern in the region between 30°N and 40°N, with wavelength of about 6600 km. Since there is no topographic forcing, these waves are free Rossby waves, which are caused and resisted by the meridional gradient of absolute vorticity due to rotation. The wavelength roughly satisfies the condition for free Rossby waves to be stationary,  $L_s = 2\pi(2u/\beta)^{1/2} \approx 7000$  km for typical values  $u = 10$  ms<sup>-1</sup> on a midlatitude  $\beta$ -plane. Animation shows that the low-pass large-scale waves are indeed quasi-stationary. The locations of weak ridges A and B match that in Figure 1, suggesting that they are the initial states of blocking A and B. The high-pass component shows transient eddy trains. Compared with observations in the real atmosphere, the eddy trains are located at lower latitudes. This is because the largest temperature gradient in the aqua-planet simulation is confined closer to the equator, as mentioned in section 2. For ridge A, strong transient eddies are located in the upstream. For ridge B, strong eddies are found around the ridge and in the downstream (There are also strong eddies in the upstream occasionally).

[9] At the maintaining stage, the low-pass field shows two well developed blocking highs. High-pass transient eddies are in the upstream of ridge A, and become weak as they approach the ridge. This is similar to the situation of North Atlantic and Pacific blockings in the real atmosphere, which lie downstream of the major storm tracks and in a

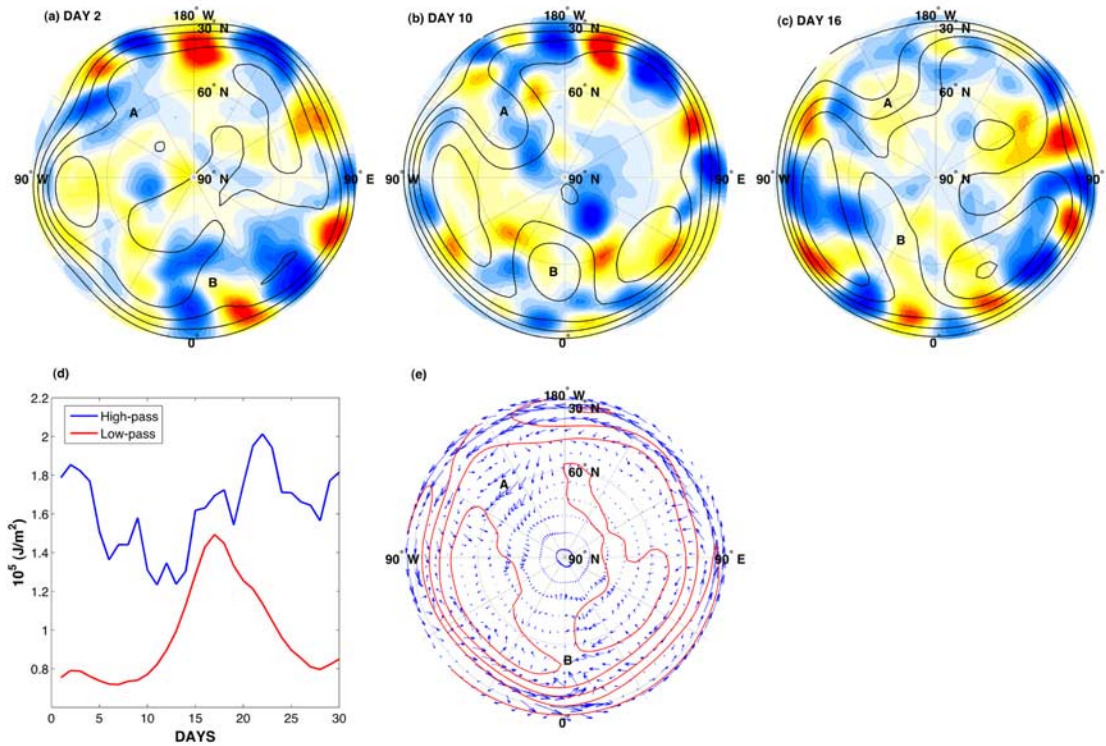


**Figure 2.** (a)–(c) High- and low-pass components of 500 hPa geopotential heights, (d) time evolution of high- and low-pass eddy kinetic energy, and (e) E-vectors over the same period as in Figure 1. A 7-day filter is applied to separating the geopotential height field. Solid contours drawn every 50 m indicate low-pass geopotential heights. Color shading indicates high-pass transient eddies, with an interval of 20 m. Following *Hoskins et al.* [1983], the low-pass component is obtained by a +1+2+1 weighting for three daily geopotential heights, and the high-pass component is obtained by a  $-1+2-1$  weighting. In Figure 2e, the arrows are E-vectors, and the superimposed contours indicate zonal winds.

region where the time-mean wave pattern tends to be characterized by ridging. However, transient eddies in the upstream of ridge B is relatively weak, and strong eddies are found only near the ridge. For both ridges, transient eddies are steered around the blocks, especially around the poleward side, and are distorted and oriented meridionally. This is also similar to the situation in the real atmosphere. It is the poleward advection of anticyclonic vorticity and upscale energy transfer by these eddies that are responsible for the maintenance of blocking anticyclones [*Hoskins et al.*, 1983].

[10] At the decaying stage, transient eddies in the upstream of ridge A become weak, suggesting that energy transfer and anticyclonic vorticity advection also become weak. Thus, the decaying of blocking A is presumably because of the weakening of the transient eddies in the upstream. For blocking B, transient eddies in the upstream are still strong, suggesting that the decaying of blocking B is caused by different reasons. One reason is probably because of its too large amplitude, which extends to the polar region and tilts toward northwest. The ridge tends to collapse after reaching its saturation value.

[11] The forcing by transient eddies on blockings can be seen from time evolution of eddy kinetic energy (KE) (Figure 2d). The decrease in high-pass KE from day 2 to 12 is accompanied by an increase in low-pass KE, with a time lag of 5 days. Low-pass KE reaches its maximum at

day 17 when both blockings remain strong and the third strong ridge develops around  $100^\circ\text{E}$ . These indicate energy transfer from transient eddies to blocking highs with time progress. The forcing of transient eddies on blockings can also be presented in terms of the “E-vector” diagnostics developed by *Hoskins et al.* [1983]. Figure 2e shows E-vectors derived from the high-pass velocity field over a 17-day sequence (between day 1 and 17). E-vectors are generally eastward in the subtropics, indicating eastward propagation of transient eddies. They are relatively large in the upstream of both blockings and show convergence in the blocking regions, which are indicative of transient eddy forcing in maintaining the blockings. E-vectors also tend to divide into two branches, pointing poleward and equatorward, respectively. This is consistent with the changing orientation of transient eddies as they move close to the two blockings. In addition to that from upstream, E-vectors in the lee sides point toward west, indicating that downstream eddies are also important in forcing blocking. In the regions with E-vector convergence, the mean flow is weakened, while in the regions with E-vector divergence the mean flow is accelerated.

[12] The essential energy source in generating and maintaining blocking is due to latitudinal temperature contrast that creates zonal-mean available potential energy (AZ), which is consequently transferred to eddy available potential energy (AE) and KE due to baroclinic instability.

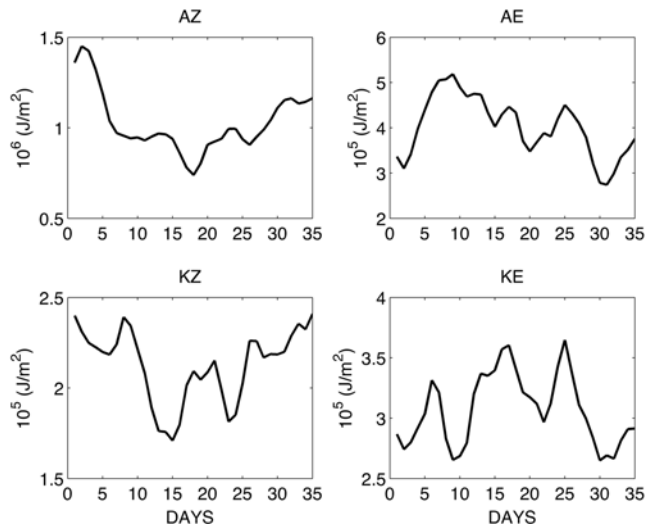


**Figure 3.** Time evolution of vertically integrated (1000–100 hPa) and area-weighted (over the zonal belt between 20°N and 80°N) energy cycle over the same period as in Figure 1: (a) zonal-mean available potential energy, (b) eddy available potential energy, (c) zonal-mean kinetic energy, and (d) eddy kinetic energy.

Energy cycles are calculated based on the equations by *Holton* [1994] and are plotted in Figure 3. AZ is large at beginning, but drops rapidly. AZ remains relatively low over day 6–27. Since there is another blocking occurring around day 25, AZ does not recover until day 30. KZ also decreases and remains relatively low over day 13–24. The decrease lags behind that of AZ by about one week. In contrast to the change in AZ and KZ, AE increases and maintains relatively high values over day 5–25, and KE also maintains high values over day 12–28. Such energy cycles are qualitatively consistent with that in the real atmosphere given by *Hansen and Chen* [1982]. It is noticed that KZ has a weak peak over day 15–23, unlike the typical case given by *Hansen and Chen* [1982] in which KZ (KE) maintains low (high) values during blocking. It is probably because of conversion from KE to KZ. One can see that the weak peak in KZ corresponds to KE decrease over day 16–22. More typical energy cycles of KE and KZ are found in different blocking episodes.

[13] A question is how frequent blockings occur in the aqua-planet simulation. To show the frequency of blockings, we use the criteria suggested by *Dole and Gordon* [1983] and *Shukla and Mo* [1983] to count numbers of blocking episodes over 10-year simulations. An anticyclone or ridge is considered a blocking if the 500 hPa geopotential anomalies at middle and high latitudes are larger than the climatological standard deviation and the anomalies persist for at least 7 days. For the aqua-planet simulation, the standard deviation for 500 hPa geopotential heights is about 140 m, close to the value of 150 m in NH spring and autumn [*Shukla and Mo*, 1983]. Figure 4 shows the histogram of blocking events as a function of anticyclone durations. The distribution is similar to that shown by *Dole and Gordon* [1983] and *Wiedenmann et al.* [2002]. There are totally 265 blocking events in NH for the 10-year simulation (the Southern Hemisphere (SH) has roughly

the same number). It is evident that blocking events are not rare. In fact, the frequency of blocking events is even slightly higher than the observed 745 events over 30 years in the NH and much higher than the 292 events over 30 years in SH [*Wiedenmann et al.*, 2002].

#### 4. Discussion and Conclusions

[14] We have shown that blocking can frequently occur in aqua-planet simulations. The simulated blockings display significant features which resemble that in the real atmosphere, such as anomalously large amplitudes, persistence, quasi-stationary behavior with occasionally westward shifting. The results suggest that blocking can form in the absence of forced large-scale waves by topography or stationary remote tropical forcing.

[15] The onset and maintenance of simulated blockings are through interaction between quasi-stationary free Rossby waves and transient baroclinic eddies. It appears that free Rossby waves in aqua-planet simulations act as forced large-scale waves in the real atmosphere in generating blocking. Quasi-stationary weak ridges set initial states for blockings. Convergence of transient-eddy fluxes leads to amplification of the ridges. Once blockings are formed, continuing convergence of transient-eddy fluxes maintains blockings against dissipation. These are consistent with the physical processes of blocking in the real atmosphere. The decaying of the two blocking episodes is due to different mechanisms. Blocking A decays because of the weakening of upstream transient eddies. Blocking B decays due to the collapse of its too large amplitude. Energy cycles show conversion from AZ to AE and KE, indicating that meridional temperature contrast is the essential energy source for blocking maintenance in the aqua-planet simulation.

[16] Such a high frequency of blockings in the aqua-planet simulation seems to contradict with the observational fact that SH has more homogeneous surface conditions and thus has weaker and less frequent blockings than NH does [*Wiedenmann et al.*, 2002]. A plausible explanation for the difference is that meridional temperature gradients in the middle and upper troposphere in the simulation are much larger than in the real atmosphere [*Neale and Hoskins*, 2001b]. Simulated tropical temperatures at 500 hPa is about

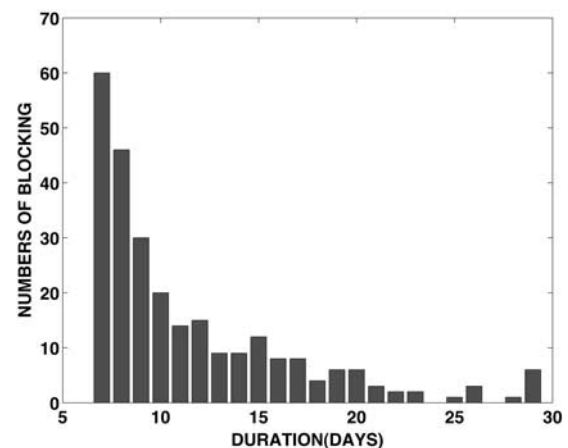


**Figure 4.** Histogram of blocking events as a function of durations for the model NH over 10-year simulations.

8°C higher than observations, while they are roughly equal at middle latitudes. The larger meridional temperature gradients lead to stronger baroclinic eddy forcing in generating blocking. Whether it is the cause for the high blocking frequency can be tested using different meridional SST profiles. This will be studied in future works. In addition, detailed diagnostics on vertical structures of blockings, upscale energy cascade and vorticity budget during blocking episodes will also be carried out.

[17] **Acknowledgments.** This work is supported by the Ministry of Education of China (106002 and 20070001002), by the NSF of China (40575031 and 40533016), and by the National Basic Research Program of China (973 Program, 2007CB411801).

## References

- Chang, E. K. M., S. Lee, and K. L. Swanson (2002), Storm track dynamics, *J. Clim.*, *15*, 2163–2183.
- Charney, J. G., and J. G. DeVore (1979), Multiple flow equilibria in the atmosphere and blocking, *J. Atmos. Sci.*, *36*, 1205–1216.
- Collins, W. D., et al (2003). Description of the NCAR Community Atmosphere Model (CAM2), <http://www.cesm.ucar.edu/models/atm-cam/docs/cam2.0>, Natl. Cent. for Atmos. Res., Boulder, Colo.
- Dole, R. M. (1986), The life cycles of persistent anomalies and blocking over the North Pacific, *Adv. Geophys.*, *29*, 31–69.
- Dole, R. M., and N. D. Gordon (1983), Persistent anomalies of the extratropical Northern Hemisphere wintertime circulation: Geographical distribution and regional persistence characteristics, *Mon. Weather Rev.*, *111*, 1567–1586.
- Egger, J., W. Metz, and G. Muller (1986), Forcing of planetary-scale blocking anticyclones by synoptic-scale eddies, *Adv. Geophys.*, *29*, 183–198.
- Feldstein, S., and S. Lee (1996), Mechanisms of zonal index variability in an Aquaplanet GCM, *J. Atmos. Sci.*, *53*, 3541–3555.
- Hansen, A. R., and T.-C. Chen (1982), A spectral energetics analysis of atmospheric blocking, *Mon. Weather Rev.*, *110*, 1146–1165.
- Holton, J. R. (1994), *An Introduction to Dynamic Meteorology*, 4th ed., Academic, New York.
- Hoskins, B. J., I. N. James, and G. H. White (1983), The shape, propagation and mean-flow interaction of large-scale weather systems, *J. Atmos. Sci.*, *40*, 1595–1612.
- Luo, D., and Z. Chen (2006), The role of land-sea topography in blocking formation in a block-eddy interaction model, *J. Atmos. Sci.*, *63*, 3056–3065.
- Mullen, S. L. (1987), Transient eddy forcing of blocking flows, *J. Atmos. Sci.*, *44*, 3–22.
- Nakamura, H., M. Nakamura, and J. L. Anderson (1997), The role of high- and low-frequency dynamics in blocking formation, *Mon. Weather Rev.*, *125*, 2074–2093.
- Neale, R. B., and B. J. Hoskins (2001a), A standard test for AGCMs including their physical parametrizations. I: The proposal, *Atmos. Sci. Lett.*, *1*, 101–107, doi:10.1006/asle.2000.0019.
- Neale, R. B., and B. J. Hoskins (2001b), A standard test for AGCMs including their physical parametrizations. II: Results for the Met Office Model, *Atmos. Sci. Lett.*, *1*, 108–114, doi:10.1006/asle.2000.0020.
- Renwick, J. A., and J. M. Wallace (1996), Relationships between North Pacific wintertime blocking, El Niño, and the PNA pattern, *Mon. Weather Rev.*, *124*, 2071–2076.
- Shukla, J., and K. C. Mo (1983), Seasonal and geographical variation of blocking, *Mon. Weather Rev.*, *111*, 388–402.
- Shutts, G. J. (1986), A case study of eddy forcing during an Atlantic blocking episode, *Adv. Geophys.*, *29*, 135–164.
- Tung, K.-K., and R. S. Lindzen (1979), The theory of stationary long waves. I: A simple theory of blocking, *Mon. Weather Rev.*, *107*, 714–734.
- Wiedemann, J. M., A. R. Lupo, I. I. Mokhov, and E. A. Tikhonova (2002), The climatology of blocking anticyclones for Northern and Southern hemispheres: Block intensity as a diagnostic, *J. Clim.*, *15*, 3459–3473.

---

Y. Hu, D. Yang, and J. Yang, Department of Atmospheric Sciences, School of Physics, Peking University, Beijing, 100871, China. (yyhu@pku.edu.cn)